1990

Edge Detection Applies to SST Fields

Jean-François Cayula

Peter C. Cornillon
University of Rhode Island, pcornillon@uri.edu

Citation/Publisher Attribution

Jean-Francois Paul Cayula, Jean-Francois Paul Cayula, Peter C. Cornillon, Peter C. Cornillon, } "Edge detection applied to SST fields", Proc. SPIE 1301, Digital Image Processing and Visual Communications Technologies in the Earth and Atmospheric Sciences, (1 November 1990); doi: 10.1117/12.21410
Available at: https://doi.org/10.1117/12.21410

PROCEEDINGS REPRINT

SPIE—The International Society for Optical Engineering

Reprinted from

Digital Image Processing and Visual Communications Technologies in the Earth and Atmospheric Sciences

18-19 April 1990
Orlando, Florida

Volume 1301

Box 10, Bellingham, Washington 98227 USA. Telephone 206/676-3290.

Edge Detection Applied To SST Fields

by

Jean-François Cayula and Peter Cornillon

Graduate School of Oceanography
University of Rhode Island
Narragansett, RI 02882

ABSTRACT

The wide availability of workstations has made the creation of sophisticated image processing algorithms economically possible. Here the latest version of an algorithm designed to detect fronts automatically in satellite-derived Sea Surface Temperature (SST) fields, is presented. The Algorithm operates at three levels: picture level, window level, and local/pixel level, much as humans seem to. Following input of the data, the most obvious clouds (based on temperature and shape) are identified and tagged so that data which do not represent sea surface temperature are not used in the subsequent modules. These steps operate at the picture and then at the window level. The procedure continues at the window level with the formal portion of the edge detection. Using techniques for unsupervised learning, the temperature distribution (histogram) in each window is analyzed to determine the statistical relevance of each possible front. To remedy the weakness related to the fact that clouds and water masses do not always form compact populations, the algorithm also includes a study of the spatial properties instead of relying entirely on temperatures. In this way, temperature fronts are unequivocally defined. Finally, local operators are introduced to complete the contours found by the region based algorithm. The resulting edge detection is not based on the absolute strength of the front, but on the relative strength depending on the context, thus making the edge detection temperature-scale invariant. The performance of this algorithm is shown to be superior to that of other algorithms commonly used to locate edges in satellite-derived SST images.

1. INTRODUCTION

Satellite-derived sea surface temperature (SST) fields are often rich in structure reflecting important underlying oceanographic processes related to eddies, currents, and regions of divergence or convergence. Many oceanographic studies that make use of satellite-derived data rely on an accurate location of edges associated with these features. To date, although it is labor intensive, the location of edges in oceanographic images has been performed subjectively by human operators. However, because of the constantly increasing amount of satellite-derived data available[10] and because computers have become faster and less expensive, there has been a rising interest in designing algorithms to automatically detect oceanographic features such as temperature fronts[11,13,16]. The primary advantage of such algorithms, aside from their speed, is that they can be designed to objectively detect fronts. In comparison, decisions by human operators are in part subjective and as a result, location of the same front will vary from day-to-day and operator-to-operator. Also, unlike subjective detection, an objective algorithm uses numerical estimates to determine the validity of a front. Consequently an objective algorithm can produce quantitative information about a front without additional computations.

Existing computer vision algorithms have been designed for purposes other than the study of oceanographic data. As a result, they often work poorly when applied to sea surface temperature fields. In this manuscript, we present a solution to the problem of objectively detecting and locating features of oceanographic interest in SST fields.

We continue our introductory remarks with a brief review of local versus regional operators and conclude them with an overview of the algorithm developed in this work. Subsequent sections deal with the details of the algorithm and a brief discussion of its application to SST fields of the western North Atlantic.

1.1. Local versus Regional Operators

To detect temperature fronts (step edges), the algorithm implemented in this study, combines algorithms operating at the local level and the regional level. The difference between local and regional algorithms is best demonstrated by example. In the case of the regional approach, the edge is defined as the (usually thin) region of separation between two compact regions of constant temperature. As a result, an edge can only be detected if two populations are found in the area being examined. For example in the one-dimensional case depicted in Figure 1.a, an edge would be detected by the regional approach because two compact populations are indeed present and well defined in the interval considered. Similarly, an edge would be detected in Figure 1.b, although the transition between the two populations is smooth. However, in Figure 1.c no edge would be detected because, aside from a few points, only one population is present. On the other hand, the local approach relies on the size and shape of the step separating the two populations. An example of such an approach is the gradient method in which a high gradient magnitude indicates the presence of an edge. Depending on the threshold used, an edge is likely to be detected in the cases shown in Figure 1.a and 1.c. However, the smoothness of the transition in Figure 1.b may prevent the detection of the edge.

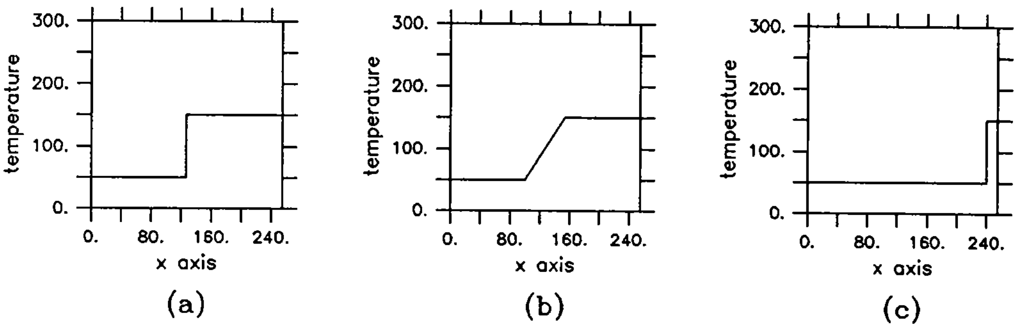

Figure 1: a–Two well defined populations. b–The smoothness of the edge can be a problem for the local approach. c–An edge is present, but one of the populations is not well defined.

Many examples of both local and regional edge detection algorithms may be found in the literature. Basic examples of local operators include the Roberts operator[12] and the Sobel operator[14]. Because these well-known operators are simple discrete approximations to the gradient, they are characterized by spurious responses when applied to noisy data. Approaches taken to remedy this problem[2] are not well suited to oceanographic data because a learning set to estimate the noise which results from variable environmental conditions such as clouds and fog[18], is not available. Another problem is that locally based algorithms using gradient operators are not scale-invariant and weak edges, no matter how well defined, are often left undetected. Methods designed to address this problem, such as the zero-crossing method[19], despite improvements[15], can still result in poor localization of edges[20].

The main problem with locally based algorithms is that they are not adaptive: they use a fixed threshold. A popular method to make vision algorithms quasi-adaptive is to segment the image in windows[8]. Then, each window can be studied separately to obtain the parameters associated with the data inside the window. Such a region based method has been used in different ways. In one algorithm[9], only the windows not containing any edges are considered to estimate the parameters of the populations in the image. These parameters are then used to grow regions and to locate edges. However, to be successful, the algorithm requires globally closed edges and this condition is not satisfied with SST data. One of the more practical algorithms[7] is derived from the observation that if an edge is present in a window, the histogram will be bimodal. It should however be noted that although the presence of an edge in a window implies a bimodal histogram, the converse is not true. This is a weakness which may arise when working with oceanographic data because clouds and water masses may not form compact populations.

1.2. Overview of the Algorithm

The algorithm discussed in this work operates at three levels: picture level, window level, and local/pixel level, much as humans seem to[11]. The flow chart of the algorithm is presented in Figure 2. Following input of the data, the most obvious clouds (based on temperature and shape) are identified and tagged so that data that do not represent sea surface temperature are not used in the subsequent modules[3,4]. These steps operate at the picture and then at the window level. The procedure continues at the window level with the formal portion of the edge detection. Using techniques for unsupervised learning[12], the temperature distribution (histogram) in each window is analyzed to determine the statistical relevance of each possible front[17,24]. To remedy the weakness related to the fact that clouds and water masses do not always form compact populations, the algorithm also includes a study of the spatial properties instead of relying entirely on temperatures. In this way, temperature fronts are unequivocally defined. Finally, local operators are introduced to complete the contours found by the region based algorithm (contour following[1,22]). It should be noted that even though local operators are used, they are used in conjunction with the window based algorithm, and so the qualities of scale invariance and of adaptivity associated with the region based approach are not lost. As a result, the algorithm takes advantage of both the regional approach and the local approach while avoiding their drawbacks.

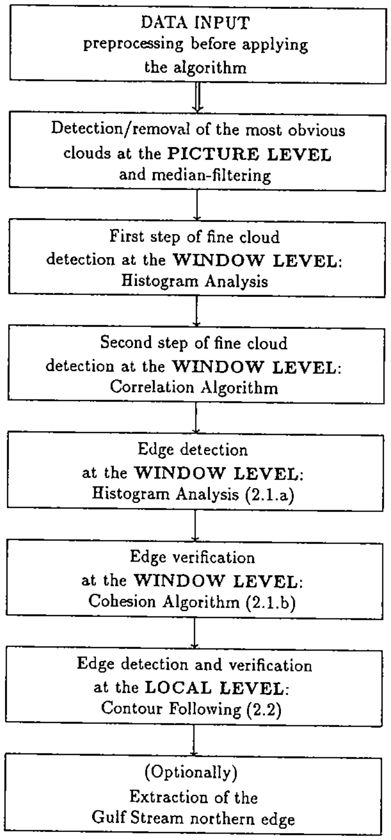
DATA INPUT
preprocessing before applying the algorithm
Detection/removal of the most obvious clouds at the PICTURE LEVEL and median-filtering
First step of fine cloud detection at the WINDOW LEVEL: Histogram Analysis
Second step of fine cloud detection at the WINDOW LEVEL: Correlation Algorithm
Edge detection at the WINDOW LEVEL: Histogram Analysis (2.1.a)
Edge verification at the WINDOW LEVEL: Cohesion Algorithm (2.1.b)
Edge detection and verification at the LOCAL LEVEL: Contour Following (2.2)
(Optionally) Extraction of the Gulf Stream northern edge

Figure 2: Flow chart of the algorithm.

2. THE ALGORITHM

As indicated above, the complete algorithm deals with both cloud and edge detection. However, because the latter is the focus of this research, only the portion of the regional-level algorithm concerned with edge detection and the local-level section will be discussed in the following. Information about the cloud detection portion of the algorithm may be found in [3,4].

2.1. Window-Level Processing

The first step of the regionally-based algorithm is to segment the entire (median-filtered) image into windows. Then each window is processed independently from the others to evaluate the probability of an edge being present in that window. Because an edge located at the boundary between two windows would escape detection, the image is segmented into overlapping windows. In the current configuration, the size of the windows has been set to 32 × 32 pixels. Such a choice in size results from a trade-off between opposing requirements. First, the data set must be sufficiently large to obtain reliable statistics. Moreover, the windows must not be too small compared to the thickness of the edge. This is due to the fact that an edge is defined as the boundary of two regions, ω_1 and ω_2, each of approximately constant temperature. If the transition between these regions occupies too much of the window, the two regions of constant temperature cannot be found and the edge is left undetected. On the other hand, by choosing a window which is too large, features that interfere with the detection of the edge may be included in the area under study. Other edges or clouds are examples of such interfering features. Although the window size and the (spatial) scale of the image are important parameters, the algorithm is robust to changes in these parameters: similar results were obtained by using 16 × 16, 32 × 32 or 64 × 64 pixels windows in processing images at scales of 1 and 2 kilometer resolution. Note that the window size is also dependent on such factors as image noise and the resolution desired for edge detection.

2.1.a. Histogram analysis

The problem addressed in this section is the detection of an edge within a given window. Because of computational considerations, only the temperature distribution (histogram) is used to determine the presence of an edge. Qualitatively, it is easy to see that if an edge is not present in the window, the histogram will likely be uni-modal. On the other hand, if an edge is present, then the histogram will be bimodal. In Figure 3, the histogram of a region containing a strong front (the window in Figure 4) is shown.

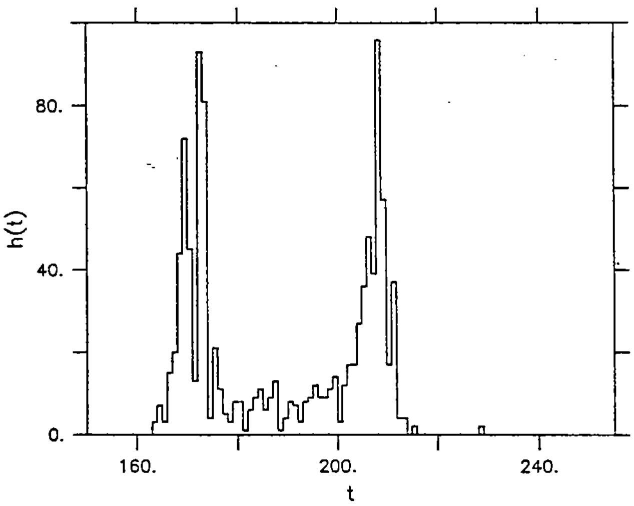

Figure 3: Histogram of a region containing a strong edge, the boundaries of the region are represented by window 1 in the image shown in Figure 4.

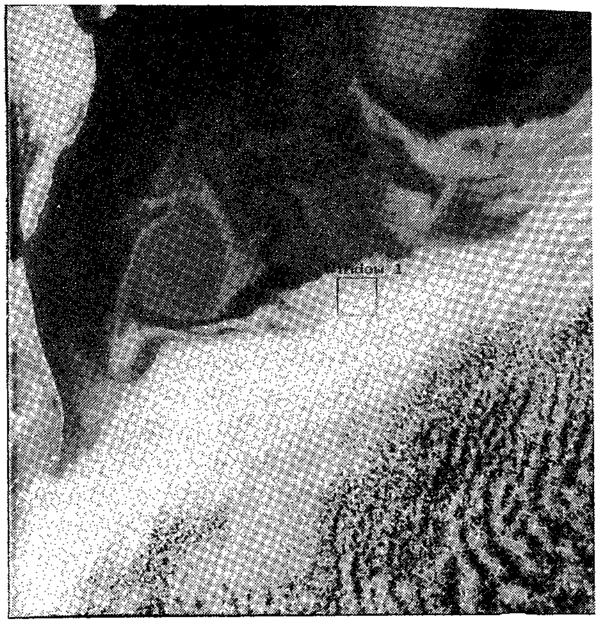

Figure 4: SST fields off Cape Hatteras, North Carolina on April 23, 1982.

The problem addressed by the analysis of the histogram is two-fold: the algorithm must determine whether one or two populations are present and, if two populations are present, a threshold must be defined to separate them. To achieve this, the algorithm first assumes that two populations are present and the parameters for the populations are computed. These estimated parameters are then used to determine if the segmentation of the data in two classes is statistically relevant. If the data in the window come from only one class, then there is no edge present in the window.

Before presenting the method used in the algorithm, the theoretical basis for the problem of unsupervised segmentation is examined. Samples from class ω_1 are defined as the cold population and samples from class ω_2 form the warm population. Let x be a sample (pixel) from the set $\mathcal{X}$ (region under study) and $t(x)$ be the temperature of the sample x. The probability density of the mixture can be expressed as:

$$p(t(x)) = \sum_{i=1}^{2} p(t(x)/x \in \omega_i)P(x \in \omega_i). \tag{1}$$

Once the parameters of the marginal densities and the *a priori* probabilities $P(x \in \omega_i)$ are determined, the validity of classifying the data in two classes versus one can be determined. If the two classes hypothesis is verified, the threshold τ that satisfies the Bayes minimum error criterion can be obtained by minimizing the probability of incorrect classification over the entire set $\mathcal{X}$ of samples:

$$P(error) = P(t(x) \geq \tau/x \in \omega_1)P(x \in \omega_1) + P(t(x) < \tau/x \in \omega_2)P(x \in \omega_2), \tag{2}$$

Exact solutions are available on occasion, in particular when the data are normally distributed[12]. However, obtaining the values of μ_i, σ_i and the *a priori* probabilities can be very complicated, requiring a large amount of computer time. Furthermore, the oceanographic data under consideration, do not seem to be normally distributed and so an exact solution may not be attainable.

The problem can be drastically simplified, however, if we assume that the probability of error associated with the Bayes minimum error threshold, equation (2), is negligible. In such a case, the overlap between the cold and the warm population is small. Once the optimal threshold is known, parameters such as the mean and the variance of each population can easily be computed:

$$\mu_1(\tau) = \frac{\sum_{t<\tau} t\, h(t)}{\sum_{t<\tau} h(t)}, \tag{3}$$

$$\mu_2(\tau) = \frac{\sum_{t\geq\tau} t\, h(t)}{\sum_{t\geq\tau} h(t)}, \tag{4}$$

$$\sigma_1(\tau) = \frac{\sum_{t<\tau}(t-\mu_1)^2 h(t)}{\sum_{t<\tau} h(t)}, \tag{5}$$

$$\sigma_2(\tau) = \frac{\sum_{t\geq\tau}(t-\mu_2)^2 h(t)}{\sum_{t\geq\tau} h(t)}, \tag{6}$$

where $h(t)$ is the value of the histogram at temperature t. Although the threshold is not known, we note that the histogram only takes a finite number of values $[0, n]$, where n is the number of quantization levels for the computer representation of the temperature. This means that τ can only take the values 1 to n. Because n is not too large ($n = 255$ for the data available to this study), one can compute an estimate of the parameters of the mixture, for every τ possible. Then, the estimated parameters can be used to maximize or minimize a given criterion over all the possible values of the threshold τ. For example, if the density function of each population is assumed to be known, the threshold τ_{best} can be chosen such that,

$$J(\tau) = \sum_{t=0}^{n}\Big(p(t/\mu_1(\tau), \mu_2(\tau), \sigma_1(\tau), \sigma_2(\tau)) - h(t)\Big)^2 \tag{7}$$

is minimized. It is also noted that the minimum value of $J(\tau_{best})$ gives an indication of the goodness of fit of the mixture density (with estimated parameters) to the histogram (estimated mixture density). Some refinements to improve the various estimates are possible, in particular, when the data are assumed to be normally distributed[17]. However, the data used in this project are not normally distributed and the hypothesis of normal distribution is implicitly rejected when the tails of the distribution are neglected.

Because a theoretically optimal criterion function may not exist and would likely require a large number of computations when it exists, it is more practical to heuristically design the criterion function. An example of heuristics that leads to a computationally simple algorithm can be obtained by expressing the total variance, S_{tot}, as the sum of two terms dependent on the threshold τ. The first term $J_e(\tau)$, represents the sum of the variances within each of the two populations that result from segmenting the region with respect to the threshold τ. We refer to $J_e(\tau)$ as the within-cluster variance and we define it as follows:

$$J_e(\tau) = S_1(\tau) + S_2(\tau), \tag{8}$$

where,

$$S_1(\tau) = \sum_{t<\tau}(t-\mu_1(\tau))^2 h(t) \quad \text{and} \quad S_2(\tau) = \sum_{t\geq\tau}(t-\mu_2(\tau))^2 h(t). \tag{9}$$

The second term, $J_b(\tau)$, represents the contribution to the total variance resulting from the separation of the two clusters:

$$J_b(\tau) = \frac{N_1 N_2}{N_1 + N_2}(\mu_1(\tau) - \mu_2(\tau))^2, \tag{10}$$

where,

$$N_1 = \sum_{t<\tau} h(t) \quad \text{and} \quad N_2 = \sum_{t\geq\tau} h(t). \tag{11}$$

Assuming that the histogram exhibits two well-defined peaks, if τ is chosen optimally most of the variance in the window will be due to the difference in temperature between the two populations. Therefore, $J_b(\tau)$ will likely be large compared to $J_e(\tau)$. On the other hand if pixels from one population are mistakenly included in the other population, some of the terms contributing to the between-cluster variance will be shifted to terms contributing to the within-cluster variance, $J_e(\tau)$. The preceding reasoning leads us to define the optimal threshold, τ_{opt}, as the value which maximizes the between-cluster variance $J_b(\tau)$. Furthermore, the ratio $J_b(\tau)/S_{tot}$ measures the proportion of the total variance due to the separation between clusters and as such gives an indication on the goodness of the segmentation. In particular this ratio, denoted $\theta(\tau)$, when evaluated at τ_{opt} indicates how good the best segmentation is. Accordingly, $\theta(\tau_{opt})$ is the criterion used to decide whether one or two populations are present. The reasoning followed to select the best threshold and determine the number of populations is only approximate but we believe that it holds in the present case because the different populations (masses of water) generally have similar variances. Although the ratio, $J_b(\tau_{opt})/S_{tot}$, is similar to such familiar statistical quantities as ρ^2 (the ratio of explained variance to total variance), it must be remembered that because the tails of the distributions in the mixture were neglected, the resulting estimates of the means and variances are biased. Furthermore, because no condition is imposed on the shape of the probability density function of each population, common statistical tests cannot be used.

Although an exhaustive analysis is not possible, the behavior of the criterion function $\theta(\tau)$ must be studied to define what criterion threshold leads to a relevant decision on the uni-modality or bimodality of the histogram. As an example, for a single normal population, the expected maximum value of the criterion function is:

$$E[\theta(\tau_{opt})] = 2/\pi \simeq 0.63. \tag{12}$$

We note that this expected value is independent of the parameters of the distribution and the size of the sample set, and has a maximum value lower than 0.7. In fact this threshold of 0.7 appears to hold whenever the histogram is clearly uni-modal: for a 32 × 32 pixels window with normally distributed data, a rough approximation[12] gives, $P(\theta(\tau_{opt}) < 0.7) \simeq 0.99$. Inversely, to show that the criterion is greater than 0.7 when two modes are present, several different bimodal distributions were simulated[3]. In light of all the cases studied, we selected 0.7 as the critical value discriminating between bimodal and unimodal distributions for use in the algorithm developed in this study. There are however potential problems associated with this critical value that require further discussion. First when the values of such parameters as the size and variance of the two populations are unequal, the algorithm performance deteriorates rapidly for a signal-to-noise ratio of less than 4. Although this requirement on the maximum amount of noise may seem very strict, it should be remembered that because the images are median filtered, if the populations are assumed to be normally distributed, a signal-to-noise ratio of 4 (or 6) would approximately correspond to a signal-to-noise ratio of only 2.3 (or 3) in the original unfiltered image[3].

It was also noted that with a signal-to-noise ratio of 4, parameter estimates are quite accurate as long as the size of the two populations does not differ by more than a factor of 3. As a result the algorithm was designed to discard any segmentation that would result in an estimated probability which does not obey the condition:

$$\hat{P}(\omega_i) \geq 0.25 \quad \text{for} \quad i = 1, 2. \tag{13}$$

Another distribution presented highlight a fundamental deficiency of any segmentation algorithm based solely on pixel values. If the data are distributed such that:

$$p(t(x)=k) = p(t(x)=k+1) = \frac{1}{2} \quad \text{for} \quad x \in \mathcal{X}, \tag{14}$$

then, by looking at the histogram of such a mixture, it seems likely that only one population is present. However, maximizing the criterion function leads to $\theta(\tau_{opt}) = 1$ (for $\tau_{opt} = k + \frac{1}{2}$), indicating that the hypothesis of two populations is highly probable. Until further information, such as limits on the possible range of the variances, is made available, an objective decision cannot be reached. In the section on post-histogram analysis, an algorithm that offers a solution to such a problem by using the spatial distribution of the data as a source of new information is discussed.

Thus far, it has been assumed that at most two populations exist in a window. Sometimes, however three populations are present. When the third population represents a small portion of the window under study, the algorithm will only detect the two principal populations. In most cases, such behavior is acceptable because the third population will likely be detected in one of the overlapping windows in which it represents a larger proportion of the data set. If the detection of three populations is required, a new criterion function $\theta(\tau_1, \tau_2)$ which would be similar to $\theta(\tau)$, could be designed. The resulting algorithm would then consist of maximizing the new criterion function for every τ_1 and τ_2 such that $\tau_1 < \tau_2$, and then, the best segmentation into three populations would have to be compared to the segmentation into two populations and to the one population case. However, for an image composed of 8-bit pixels, the computational cost can be multiplied by as much as 128. For satellite-derived fields of 1 km resolution, overlapping 32 x 32 pixel windows were sufficiently small to eliminate the multiplicity of fronts within a given window as a serious problem; this providing that fronts associated with land or clouds are removed prior to applying the edge detection algorithm.

2.1.b. Cohesion Algorithm

By neglecting to take into consideration the spatial distribution of the data in the previous section, a large amount of information was left unused. For example, in the case described by equation (14), if all the pixels of value k form a compact region, then the hypothesis of a front being present in the area would definitely seem more legitimate. On the other hand, if pixels of any value are uniformly distributed throughout the window, then the hypothesis that a front exists in the window would be invalidated. Whenever the histogram indicates the presence of two populations, the spatial distribution of the data should be examined to see if a front is present or if the bimodal distribution is simply a result of an erratic temperature pattern. In studying SST fields, the problem of a bimodal distribution resulting from scattered clouds over water with no front present is encountered on occasion. This problem may also occur when the sensor has intermittent noise as was the case with some NOAA-6 data.

In general, when two populations have been detected by histogram analysis, the segmentation obtained by thresholding the data at τ_{opt} will lead to spatially compact populations if a front is actually present. To test for such spatial compactness, an algorithm that measures the cohesion of each population has been designed. This algorithm is only applied when two populations, A and B, have been detected in the histogram analysis. Populations A and B are defined such that, for a pixel x with temperature $t(x)$:

$$t(x) \leq \tau_{opt} \quad \Rightarrow \quad x \in A \qquad \text{and} \qquad t(x) > \tau_{opt} \quad \Rightarrow \quad x \in B. \tag{15}$$

The cohesion coefficients for populations A and B, and for the entire data set are defined as follows:

$$C_A \equiv \frac{R_A}{T_A}, \tag{16}$$

$$C_B \equiv \frac{R_B}{T_B}, \tag{17}$$

$$C \equiv \frac{R_A + R_B}{T_A + T_B}. \tag{18}$$

where T_A, the total number of comparisons between center pixels belonging to population A and neighbor pixels belonging to either population, is given by:

$$T_A = \left| \{ (x, y), \quad \text{such that} \quad y \in (\mathcal{N}(x) \cap \mathcal{X}), \quad \forall x \in A \} \right|, \tag{19}$$

and R_A, the total number of comparisons between center pixels and neighbors that both belong to population A, is given by:

$$R_A = \left| \{ (x, y), \quad \text{such that} \quad y \in (\mathcal{N}(x) \cap A), \quad \forall x \in A \} \right|. \tag{20}$$

R_B and T_B are similarly defined by substituting B for A in equations (19) and (20) and $|\cdot|$ is defined as the cardinality of the set. For reasons of computational economy and simplicity, only the first neighbors of a given pixel are used to evaluate the cohesion. If $x_{i,j}$ is the center pixel, the set of first neighbors is $\mathcal{N}(x_{i,j}) = \{x_{i,j+1}, x_{i,j-1}, x_{i+1,j}, x_{i-1,j}\}$.

High cohesion means that for a given pixel which is not close to the edge, neighboring pixels are likely to belong to the same population. This implies that the spatial segmentation of the area into populations A and B is validated. Inversely, low cohesion means that there is a non negligible probability that a given pixel has neighbors from a different population and so the presence of the front detected by the histogram analysis is improbable. For a checker-board pattern the three cohesion coefficients are zero and for an image with the bottom half coming from one population and the top half coming from the other population, the cohesion coefficients will tend to unity when the effects at the edge between the populations are neglected. As a matter of fact, when the noise is assumed independently distributed, the following equation can be derived[3,4]:

$$C \simeq 1 - 2P(error). \tag{21}$$

A threshold of 0.92 for C and 0.90 for C_A and C_B was chosen in this work to eliminate edges resulting from noisy distributions, i.e., if C is less than 0.92 or C_A or C_B was less than 0.90, the segmentation is discarded as unreliable.

Although the actual algorithm takes into account the presence of an edge in the window, there are cases for which the contribution of the edge to the estimate of the cohesion may be different from the contribution of a straight edge. It should be noted however, that if $P(error)$ is zero, the threshold on C can accommodate a front which is about three times longer than a straight front. This trade-off between length of the front and signal-to-noise ratio is actually an interesting property of the algorithm. Because SST fronts are generally associated with mesoscale oceanographic processes, the fronts are expected to be fairly straight (or at least smooth) on the scale of the 32 x 32 pixel windows. On the other hand, rugged edge contours are most often found at the boundary of clouds or of land areas, i.e., they are not edges between water masses. Because long (not straight) edges often are not valid temperature fronts, they are less reliable than shorter (straight) fronts. Accordingly, the condition on the minimum signal-to-noise ratio should be made more stringent for accepting long edges as valid temperature fronts. In summary, it can be seen that the cohesion algorithm estimates both the length of the edge contour in a window and the compactness of each population. Although the edge effects on the cohesion could be reduced, physical considerations of the problem justifies the approach used to estimate the cohesion coefficients.

2.1.c. Location of Edge Pixels

The window-level algorithms discussed above were designed to detect and confirm the presence of an edge in each individual window. The last step in this process is to locate the edge pixels in the windows where the presence of a front was detected and confirmed. The output of this algorithm is an edge image in which any pixel which is not an edge pixel is set to a digital count of zero. Pixels that are determined to be edge pixels are set to a value equal to the temperature threshold obtained by histogram analysis. Using the indicator function $\Omega(x)$ such that,

$$\forall x \in \mathcal{X}, \Omega(x) = \begin{cases} 0, & \text{if } x \in A; \\ 1, & \text{if } x \in B, \end{cases} \tag{22}$$

an edge pixel can be simply expressed:

$$\begin{aligned} &\forall x \in \mathcal{X}, \quad \text{if} \quad \exists y \in \mathcal{N}'(x), \quad \text{such that} \quad \Omega(x) \neq \Omega(y), \\ &\qquad \Longrightarrow \quad x \quad \text{is an edge pixel.} \end{aligned} \tag{23}$$

2.2. Local-level processing

The edge image obtained by window level processing does not really contain edges, but independent edge pixels. Because oceanographers are interested in studying the statistics associated with a temperature front, the edge image is inadequate, and further processing is required to link the independent edge pixels so that they form continuous contours. For this reason, a contour following algorithm (local level processing) is included to complete the algorithm for frontal detection. Basically the algorithm is a directional contour following one, meaning that points are added to the contour provided that the direction of the contour does not change by more than 90 degrees in 5 pixels. Note that when no previously detected edge pixels can be added to the contour, the algorithm uses local properties of the gradient field to add new edge elements.

A few of the problems that are associated with the edge image obtained by the window level algorithm can be corrected at the local level by a contour following algorithm. For example, some fronts may have been partially missed because more than one front is present in the window. However, if the fronts are separated by more than a few pixels, the local level algorithm will have no difficulty continuing the front since it only relies on the first neighbors of the last edge pixel to find a new edge pixel to add to the existing contour. A second problem which is often encountered in the edge image, is that there may exist isolated edge pixels. This effect is mainly due to the fact that $P(error) \neq 0$. By imposing a minimum length for a valid contour, isolated points can be removed from the edge image. In the present version of the program, the minimum length of a contour is 15 pixels.

3. VALIDATION

To evaluate the performance of the edge detection algorithm, it was applied to a set of 98 satellite (NOAA-7) derived SST fields used in a previous comparative study[11]. Figure 5 shows one of the images (Figure 4) after processing. In the previous study, the location of the northern edge of the Gulf Stream off Cape Hatteras, determined subjectively from satellite imagery by a trained analyst, was compared to the location of the Gulf Stream determined from inverted echo sounders (IES) moored on the sea floor. The position of the Gulf Stream determined from IES's corresponds to the surface projection of the 15°C isotherm at 200 meters, T_{15}, the generally accepted definition of the northern edge. A detailed description of the inverted echo sounders can be found in[6]. For the present purpose, it is sufficient to note that three inverted echo sounder lines were available for the period covered by the images used here. To compare the position of the northern edge of the Gulf Stream located by the edge detection algorithm with the IES data, x_{SAT} is defined as the intersection of an IES line with the temperature front (if it exists) located by the edge detection algorithm and x_{IES} denotes the location of the intersection of T_{15} with the IES line.(Watts and Johns[23] have estimated that the standard error associated with the IES location of T_{15} compared to the location determined by XBT (expendable bathy thermograph) is about 5 km.)

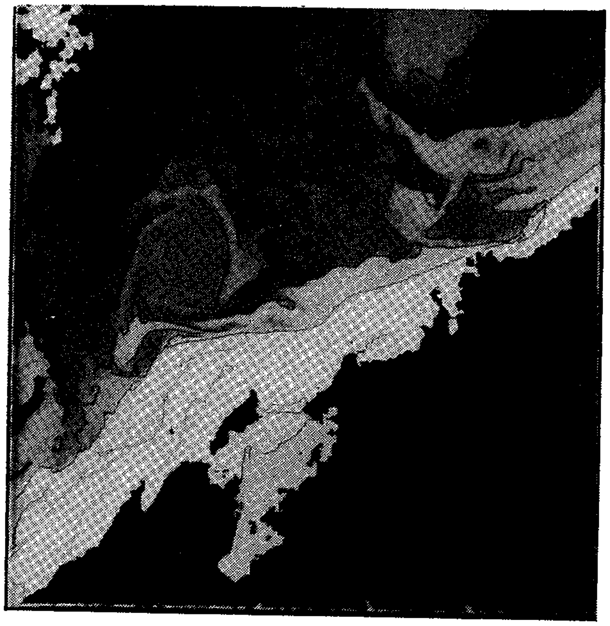

Figure 5: SST fields off Cape Hatteras with clouds zeroed out and edges overlaid (thin black lines).

To compare the satellite-derived Gulf Stream edge with the IES-derived path, statistics related to the separation of x_{SAT} and x_{IES} are generated. The distance $|x_{SAT} - x_{IES}|$ corrected for the fact that the Gulf Stream does not in general cross the IES line orthogonally is the variable used in the comparison. Because isotherms intersecting the sea surface are not vertical and because the surface projection of T_{15} is being compared with the surface front, a mean offset between the two is expected. This offset is given by:

$$m_{SAT-IES_\perp} = \frac{1}{N} \sum_{x_{SAT}/Q_f \geq q} \cos(\theta)(x_{SAT} - x_{IES}), \qquad (24)$$

where Q_f is a quality parameter, that permits the selection of the best N edges to compute the statistic. The figure of merit used to evaluate the edge detection algorithm is the scatter about the mean offset given by:

$$\sigma^2{}_{SAT-IES_\perp} = \frac{1}{(N-1)} \sum_{x_{SAT}/Q_f \geq q} \Big(\cos(\theta)(x_{SAT} - x_{IES}) - m_{SAT-IES_\perp}\Big)^2, \qquad (25)$$

where θ is the angle between the normal to the Gulf Stream edge and the IES line. In obtaining these values it is noted that one IES line may intersect several edges identified in the satellite imagery as being associated with the Gulf Stream. In such cases, only the warmest southern-most intersection is used in the comparison.

In Table 1, the edge detection algorithm (**alg**), the subjective detection (**sub**), the gradient method (**grd**) and the skew method (**skw**), (where the last two methods are objective edge detection algorithms used in the previous study[11]) are compared. Subjective detection means that an analyst manually located the northern edge of the Gulf Stream. On the other hand, the gradient method is an automated approach that relies on the Sobel operator[12]. The skew method consists of computing the skew of the data in a 7 x 7 pixel window and detecting an edge whenever the skew changes sign. Because the different methods operate differently, they assign different quality factors for the same edges: the quality factor is different if the edge is studied globally, regionally or locally. As a result, quality factors for different methods are not directly comparable and Table 1 is structured so that on a particular row, the bias and standard deviation associated with each method are given as a function of the number N of intersections, between IES lines and the Gulf Stream northern edge, which satisfy a minimum quality factor. The variations in the value of N on a particular row are not significant and are simply due to the fact that N is not a continuous function with respect to Q_f.

Table 1: Comparative results of the edge detection algorithm (**alg**), the subjective detection (**sub**), the skew method (**skw**) and the gradient method (**grd**). N is the number of intersections between the IES lines and the selected Gulf Stream fronts for those edge points which satisfy a minimum quality factor. When the minimum quality factor decreases, N increases since intersection points, which are not as reliable (lower quality factor), are selected. *The Gulf Stream northern edge was automatically selected among all the detected edges.

N				$m_{SAT-IES_\perp}$				$\sigma_{SAT-IES_\perp}$			
alg	sub	skw	grd	alg	sub	skw	grd	alg	sub	skw	grd
39*	45	49	42	-9.26	-13.32	-21.02	-23.58	14.12	13.29	20.90	21.87
87*	80	82	90	-11.08	-13.52	-18.94	-23.97	15.65	13.46	18.40	22.48
110*	113	110	109	-12.50	-13.59	-17.37	-24.50	15.61	14.62	18.97	21.92
131*	141	131	126	-14.18	-13.80	-16.91	-25.56	17.17	14.50	18.14	22.40
196	226	199	181	-12.69	-12.53	-18.29	-25.70	15.68	14.91	18.71	23.63

In comparing the results in Table 1, one notes the following: first, subjective detection leads to the lowest scatter about the mean and as a result, it is still the most accurate method to locate the northern edge of the Gulf Stream from satellite-derived images. However, scatter for temperature fronts obtained with the edge detection algorithm is very close to that obtained subjectively. The other methods lead to $\sigma_{SAT-IES_\perp}$'s which are larger than the $\sigma_{SAT-IES_\perp}$ associated with the subjective method or with the edge detection algorithm. Second, the mean offsets associated with the edge detection algorithm and the subjective method are the smallest observed. This means that the warmest, southern-most front being detected is further to the south, i.e., closer to T_{15}. Indeed, one can often detect two fronts in the region of the Gulf Stream northern edge: a first and weaker front between warmer and warm waters, and a second and stronger front between warm and cold water. It is the first front that this edge detection algorithm and the analysts are able to detect, while the gradient and skew methods will in general detect only the stronger front which is farther north.

The processing time required by the edge detection algorithm varies from image to image. On the set of the 98 images, an average of 3 minutes of μVax III CPU-time was used to process each image. The result of a comparative study[5] indicates that the edge detection algorithm while requiring at most one quarter of the computing time, performs at least as well as the algorithm (based on a local level approach) described in[16]. As a matter of fact, it seems that such a multilevel approach is generally preferable to a single level approach[5,21].

4. SUMMARY

We have presented an algorithm which is able to detect edges reliably without intervention from a human operator. To accomplish this task the algorithm operated at different levels to detect and differentiate between true and false edges.

For comparison purposes, the algorithm was applied to a test set of 98 sea surface temperature images to detect the northern edge of the Gulf Stream. For this data set, the algorithm was shown to perform better than automated methods previously used to detect the edge of the Gulf Stream from satellite-derived sea surface temperature fields: the algorithm successfully detected valid temperature fronts and ignored false edges. Furthermore, the algorithm produced statistics about the temperature fronts that are useful in the subsequent analysis of these fronts. Although the comparative evaluation has been performed on Gulf Stream edges, it is assumed that the algorithm performs equally well on other SST fronts such as those associated with rings, the subtropical convergence, the shelf/slope fronts, etc.

5. ACKNOWLEDGMENTS

The image-processing software was developed by R. Evans, O. Brown,J. Brown and A. Li at the University of Miami under Office of Naval Research funding. The continuing support of the Miami group is gratefully acknowledged.

This research project was funded by the National Aeronautics and Space Administration under contract number NAGW-858.

6. REFERENCES

1. D.H. Ballard and C.M. Brown, *Computer Vision*, Englewood cliffs, NJ: Prentice-Hall, 1982.
2. J.F. Canny, "A Computational Approach to Edge Detection," *IEEE trans. on Pattern Analysis and Machine Intelligence*, vol. PAMI–8, pp. 679–699, 1986.
3. J.-F. Cayula, *Edge Detection for SST Images*, M.S. Thesis, Department of Electrical Engineering, University of Rhode Island, 1988.
4. J.-F. Cayula and P. Cornillon, "Edge Detection Algorithm for SST images," *IEEE Trans. on Geoscience and Remote-Sensing*, (submitted), 1990.
5. J.-F. Cayula, P. Cornillon, R. Holyer and S. Peckinpaugh, "Comparative Study of Two Recent Edge Detection Algorithms Designed to Process SST Fields," *IEEE Trans. on Geoscience and Remote-Sensing*, (submitted), 1990.
6. G. Chaplin and D.R. Watts, "Inverted Echo Sounder development," *Ocean '84 Conference Record*, vol. 1, pp. 249–253, 1984.
7. C.K. Chow and T. Kaneko, "Automatic Boundary Detection of the left Ventricle from Cineangiogram," *Comput. Biomed. Res.*, vol. 5, pp. 388–410, 1972.
8. F.S. Cohen and J.-F. Cayula, "3-D Object Recognition from a Single Image," *proceedings of the 3rd SPIE Conf. on Robot Vision and Sensory Controls*, pp. 7–15, 1984.

9. F.S. Cohen and Z. Fan, *Unsupervised Textured Image Segmentation*, Department of Electrical Engineering, University of Rhode Island, Technical Report 86–1, 1986.
10. P. Cornillon, C. Gilman, L. Stramma, O. Brown, R. Evans and J. Brown, "Processing and Analysis of Large Volume of Satellite-Derived Thermal Infrared Data," *Journal of Geophysical Research*, vol. 92, pp. 12993–13002, 1987.
11. P. Cornillon and D.R. Watts, "Satellite Thermal Infrared and Inverted Echo Sounder Determination of the Gulf Stream Northern Edge," *Journal of Atmospheric and Oceanic Technology*, vol. 4, pp. 712–723, 1987.
12. R.O. Duda and P.E. Hart, *Pattern Recognition and Scene Analysis*, New York,NY: John Wiley and Sons, 1973.
13. D.J. Gerson and P. Gaborski, "Pattern Analysis for Automatic Location of Ocean Fronts in Digital Satellite Imagery," U.S. Naval Oceanographic Office, TN 3700–65–77, Oct. 1977.
14. E.L. Hall, *Computer Image Processing and Recognition*, New York, NY: Academic Press, 1979.
15. R.M. Haralick, "Digital Step Edges from Zero-crossing of Second Directional Derivative," *IEEE trans. on Pattern Analysis and Machine Intelligence*, vol. PAMI–6, pp. 58–68, 1984.
16. R.J. Holyer and S.H. Peckinpaugh, "Edge Detection Applied to Satellite Imagery of the Oceans," *IEEE Trans. on Geoscience and Remote-Sensing*, vol. GE–27, pp. 46–56, 1989.
17. J. Kittler and J. Illingworth, "Minimum Error Thresholding," *Pattern Recognition*, vol. 19, pp. 41–49, 1986.
18. D.A. Landgrebe and E. Malaret, "Noise in Remote-Sensing Systems: the effect on classification error," *IEEE trans. on Geoscience and Remote-Sensing*, vol. GE–24, pp. 294–301, 1986.
19. D.C. Marr and T. Poggio, "Theory of Edge Detection," *Proc. Roy. Soc. London*, vol. B 207, pp. 187–217, 1980.
20. W.S. Nalwa and T.O. Binford, "On Detecting Edges," *IEEE Trans. on Pattern Analysis and Machine Intelligence*, vol. PAMI–8, pp.699–714, 1986.
21 T. Pavlidis and Y.-T. Liow, "Integrating Region Growing and Edge Detection," *IEEE trans. on Pattern Analysis and Machine Intelligence*, vol. PAMI–12, pp. 225–233, 1990.
22. P. Seitz and P. Rüegsegger, "Fast Contour Detection Algorithm For High Precision Quantitative C.T.," *IEEE trans. on Medical Imaging*, vol. MI–2, pp. 136–141, 1983.
23. D.R. Watts and D.R. Johns, "Gulf Stream meanders: Observations on propagation and growth," *Journal of Geophysical Research*, vol. 87, pp. 9467–9476, 1982.
24. J.S. Weszka, "A Survey of Threshold Selection Techniques," *Computer Graph. Image Proc.*, vol. 7, pp. 259–265, 1978.